

Optoelectronic computation of waveletlike-based features

George W. Rogers

Jeffrey L. Solka

Carey E. Priebe

Department of the Navy

Naval Surface Warfare Center, Dahlgren

Division

Code K12

Dahlgren, Virginia 22448-5000

Harold H. Szu

Department of the Navy

Naval Surface Warfare Center

Code R44

10901 New Hampshire Avenue

Silver Spring, Maryland 20903-5000

Abstract. We describe an optoelectronic system to extract gray-scale texture features. These systems utilize a nonlinear resistive grid to perform a 2-D pseudowavelet transform of the optical input image. Texture features are computed using first- and second-order variance estimates of the transform coefficients. Some preliminary results are presented that demonstrate the natural segmentation that the nonlinearity provides at the boundary of two dissimilar textures and the utility of the extracted features for texture discrimination.

Subject terms: wavelet transforms; electronics; optics; texture; discrimination; segmentation.

Optical Engineering 31(9), 1886-1892 (September 1992).

1 Introduction

Given a gray scale or color image, the focus of attention is usually on a particular area. One way to accomplish this is to segment the image into various regions based on texture. This selective segmentation process has applications to both medical and satellite image processing. In this paper, we detail an approach to this selective segmentation process based on features extracted from a set of analog-computed pseudowavelet coefficients.

The silicon retina of Mead¹ displays many features of human retinal processing. Two key features of interest here are the optical input to the silicon retina chip and the center surround response of each node in the retina that is reminiscent of a Morletlike mother wavelet. This center surround response, which is similar to the difference of Gaussians, is accomplished by differencing the input at a pixel with a local average computed via an analog resistive grid. In this paper, we propose an optoelectronic system for performing resistive grid-based wavelet transformations. We include an example where the multiresolution wavelet coefficients² have been further processed to produce local variance and variance of variance features, which can be used to perform texture discrimination. The twin advantages of this hybrid approach are the near real-time processing to obtain wavelet coefficients and/or texture features and the nonlinear data-driven nature of the effective wavelets produced by a resistive grid composed of nonlinear components.

2 Background

As an outgrowth of previous work in texture discrimination based on fractal dimension-derived power law features,^{3,4} we have recently begun looking at using a (hypothetical) silicon retina to do image preprocessing for texture analysis. There are twin motivations for this line of investigation.

First and foremost, the texture discrimination ability of retinal-based biological systems provides a working prototype for this approach. Second, optoanalog implementation of our hypothetical retina offers the potential of parallel preprocessing. The postprocessing is based on well-understood parametric and nonparametric statistical techniques.⁵ This permits an analysis of the contributions of individual features produced in the preprocessing and gives us a capability to follow an "evolutionary" or experimental approach with our silicon retina model. We can delete features that do not perform, while trying variations on good features, or using new features altogether. Central to our model is the set of nonlinearities encountered in analog VLSI implementations as well as in biological systems. These nonlinearities are crucial, for example, to both segmentation and the prevention of feature contamination between disparate texture types.

We begin with a brief review of the properties of the 1-D resistive grid. Figure 1 displays a nonlinear resistive grid.¹ Given a function $f(x): R \rightarrow R$ by associating an input x bin with each node of the network, we may map a set of sampled functional values $\{(x_i, y_i) : 1 \leq i \leq M\}$ into the resistive grid by assigning for bin i an input voltage V_i proportional to y_i when x_i falls in the i 'th bin. In this manner, a discrete approximation f^{RG} to the convolution of f with an exponential kernel is obtained. For the in-line horizontal resistor circuits, it can be shown that $I = I_{\text{sat}} \tanh[(V_1 - V_2)/2]$. The voltage V_i at the i 'th node of the grid is given by solving

$$G(V_i^n - V_i) + (V_i - V_{i-1})/R_{i-1} + (V_i - V_{i+1})/R_i = 0.$$

In this equation, the nonlinear resistance of the i 'th horizontal resistor is given by

$$R_i = \frac{R_0[(V_{i+1} - V_i)/2]}{\tanh[(V_{i+1} - V_i)/2]},$$

and the discrete convolution value of our function at the i 'th bin f_i^{RG} is just the output voltage V_i of the i 'th node.

Paper WT-008 received April 1, 1992; revised manuscript received June 12, 1992; accepted for publication June 25, 1992.
©1992 Society of Photo-Optical Instrumentation Engineers. 0091-3286/92/\$2.00.

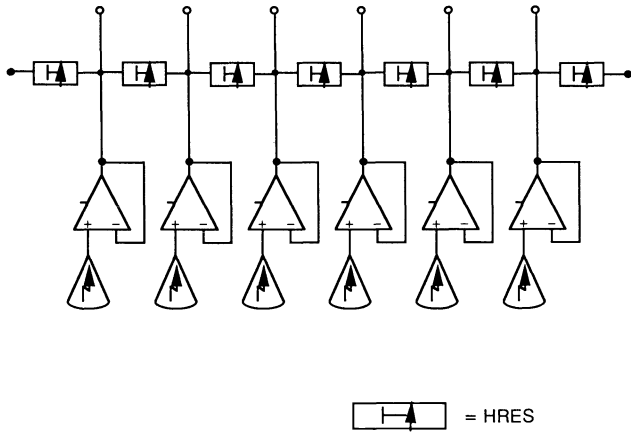


Fig. 1 Nonlinear resistive grid with optical input. The bias circuit associated with each node is not shown.

Our (hypothetical) silicon retina is centered on the use of 2-D resistive grids with orthogonal (four nearest neighbor) geometry. In a manner analogous to the 1-D case, the 2-D resistive grid functions to smooth the input in a linear or (of interest to us) a nonlinear fashion. In its linear version, the resistive grid smooths the inputs to produce an output that corresponds approximately to the convolution of the input image with an exponential kernel with a characteristic length or kernel size we denote by L_k or, equivalently, by an associated scale ϵ_k .

Let $f: \mathbb{R}^2 \rightarrow \mathbb{R}$ be the function that produces our 2-D input image defined on a discrete (pixel) array. Further, let $R_\epsilon(f): \mathbb{R}^2 \times \mathbb{R} \rightarrow \mathbb{R}^2 \times \mathbb{R}$ be the resistive grid transform of f at scale ϵ . Suppose that we compute $R_\epsilon(f)$ for n different scales: $R_2^0(f), R_2^1(f), R_2^2(f), \dots, R_2^{n-1}(f)$. Notationally, we let $L_\beta = R_2^{\beta-1}(f)$. The L_β can be thought of as functional estimates at different levels of smoothing. Next, we compute a set of features for each pixel:

$$F_\alpha = R_2^{\alpha-1}(f) - R_2^\alpha(f) = L_\alpha - L_{\alpha+1}, \quad \alpha = 1, \dots, n-1.$$

We now have a set of $n-1$ features defined at each array or grid (pixel) point that corresponds to a difference of kernels of different characteristic scales. Figure 2 details the architecture of the device that computes these features in the case of $n=4$. It utilizes optical components for input and image passing, multiple resistive grids for convolution computation, and a digital pixel on pixel subtraction process to produce the final wavelet coefficients. These are the (non-linear) resistive grid analogs of the difference-of-Gaussian wavelet basis. Thus, at each pixel, we have the first $n-1$ coefficients of a wavelet (or pseudowavelet) basis with the F_α being the coefficient arrays. In contrast to standard wavelet techniques using power of two sampling rates, we fully sampled the wavelet coefficient network at each scale value. This produces a set of wavelet functions that is overdetermined, i.e., nonorthogonal.

Now that we have these pseudowavelet coefficients, how do we use them to compute texture features? Previous work of Mallat² has suggested a correspondence between the texture primitives or textons of Julesz⁶ and the functions in a wavelet orthonormal basis. These textons, like wavelets, have a particular spatial orientation and a narrow frequency

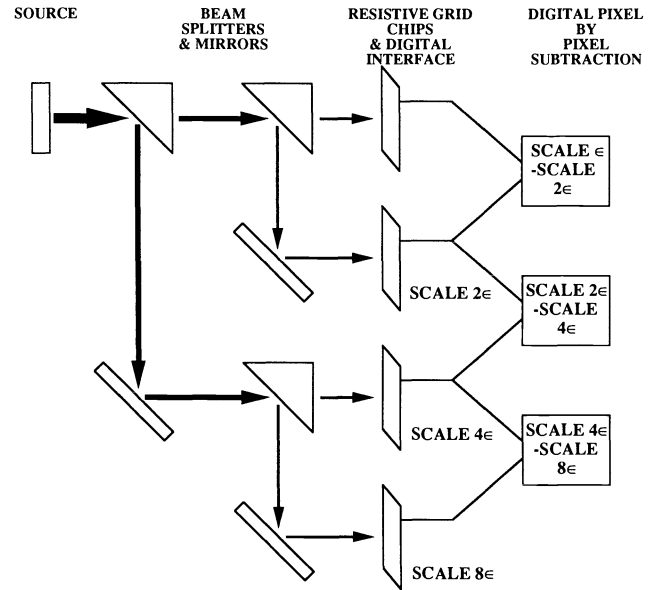


Fig. 2 Hybrid optical/analog/digital architecture for near real-time nonlinear wavelet transform. Focusing lenses are not shown for simplicity.

tuning. Work by Caeli⁷ has suggested that the outputs from these textons can best be used for texture discrimination by computing local estimates of energy. We need to estimate the local energy via our resistive grid framework.

Mead¹ has demonstrated the feasibility of performing half- and full-wave rectification in analog VLSI. An obvious feature to compute using the twin elements of resistive grids and full-wave rectifiers is a mean variance of the pseudo-wavelet coefficients as a function of scale. The goal is to compute local energy features that are relatively texture invariant. We compute these variance features ν_α as follows:

$$\nu_\alpha = R_2^{\alpha+\tau} [|F_\alpha - R_2^\alpha(F_\alpha)|].$$

Here $\tau \{1, 2, \dots\}$ is chosen to smooth these variance estimates—essentially, this last smoothing is analogous to basebanding on some carrier frequency.

This gives a set of additional features for each array location (pixel) that gives a measure of the variance of the difference of kernel features for the different scales. This set of steps can be repeated (iterated) using ν_k as input (instead of F_k) to produce a set of second-order variances ν_{kk} . Thus, we have a truncated double expansion in pseudo-wavelet coefficients and orders of variance of these coefficients, for each array location or pixel.

3 Results

In this section we discuss the linear version of our functional estimation technique along with some nonlinear simulation results. A full analytical treatment of the nonlinear theory is beyond the scope of this document. For analytical purposes, consider a linear approximation to our functional estimation technique. Call the exponential function $\phi(x)$ (Fig. 3), obtained from the resistive grid, our scaling function. We then have as our mother wavelet $\psi(x)$ the difference of exponentials depicted in Fig. 4. Figure 5 gives $\psi(x)$ at three different scale values. The effect of the nonlinearity

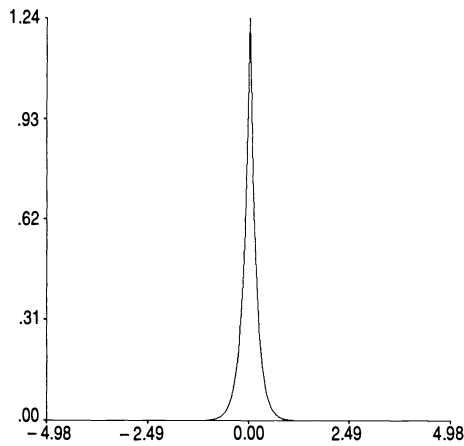


Fig. 3 Scaling function for a 1-D resistive grid with linear components.

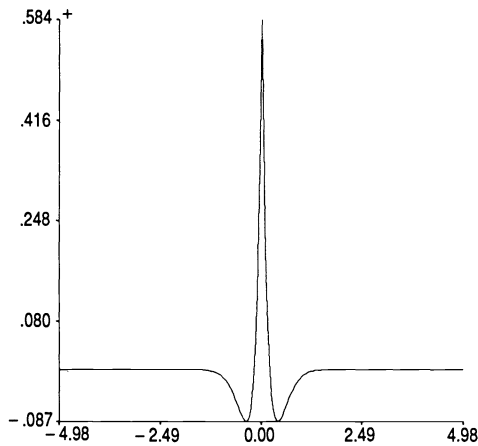


Fig. 4 Mother wavelet $\psi(x)$ for a 1-D resistive grid with linear components.

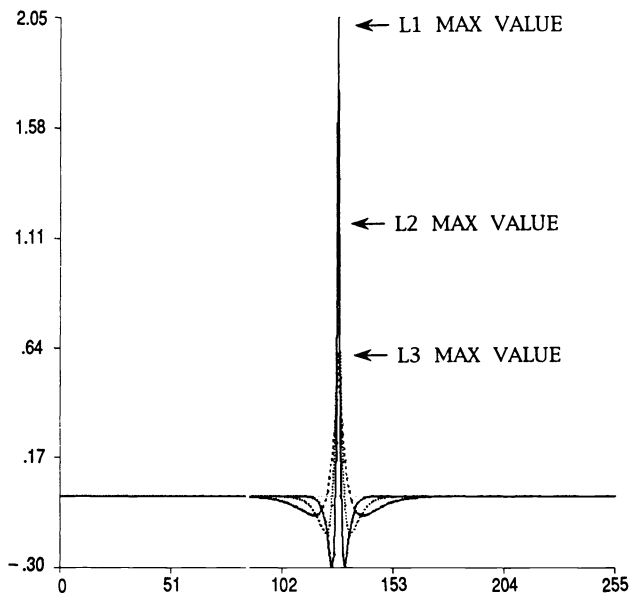
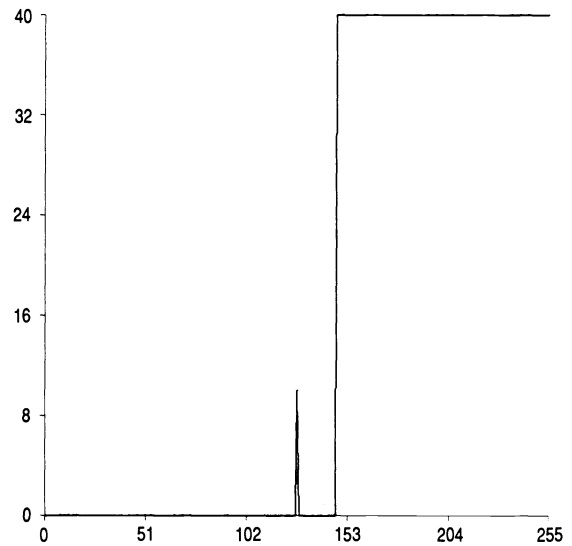
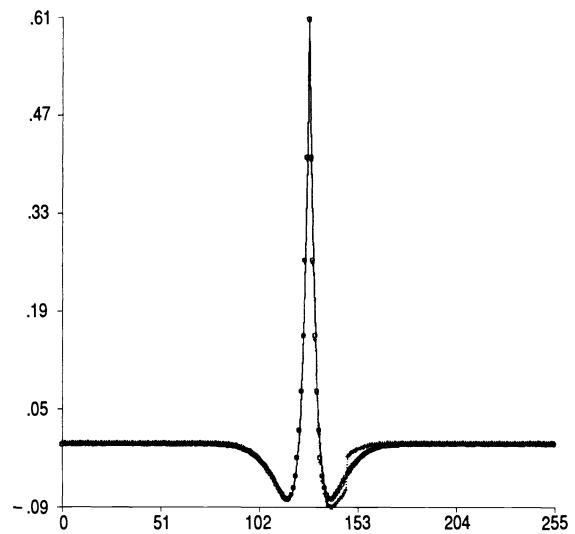


Fig. 5 One-dimensional resistive grid wavelets at three increasing scales.



(a)



(b)

Fig. 6 (a) Nonlinear 1-D resistive grid input: The grid is allowed to come to equilibrium with the step function input, then resistances are held fixed while the spike is input and (b) the effective resultant linear and nonlinear wavelet for the spike component of the total input shown in (a). The nonlinear response strongly damps the wavelet amplitude at a contrast boundary.

of the (simulated) analog VLSI implementation on this wavelet is depicted in Figs. 6(a) and 6(b). Figure 6(a) shows the discontinuous input, while Fig. 6(b) compares the $\psi(x)$ function corresponding to the linear case and the nonlinear theory. The effect of this adaptive wavelet amounts to a segmentation effect in the case where a sharp discontinuity exists (an edge) in the input, such as in Fig. 6(a). That these nonlinear effects allow for an automatic segmentation has been demonstrated previously in the ability of the resistive grid kernel estimator to model discontinuities in probability density functions while maintaining an otherwise smooth estimate (see Figs. 7 and 8).⁸

Previous work has detailed the application of wavelets to image segmentation.^{9,10} The resistive elements in the

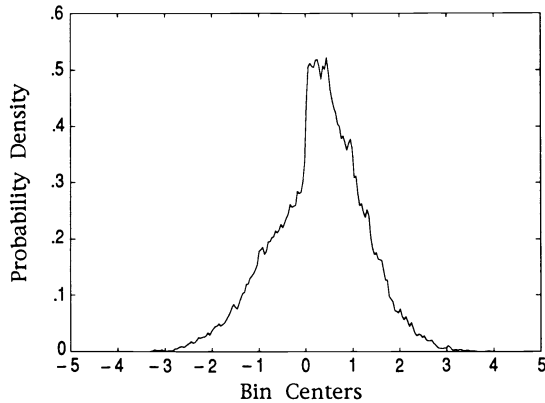


Fig. 7 Linear resistive grid kernel approximation of a probability density function that contains a jump discontinuity.

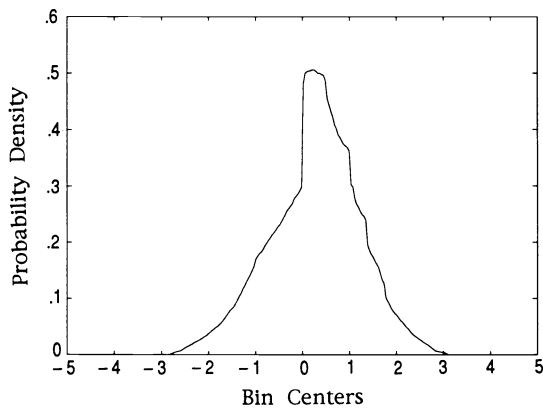


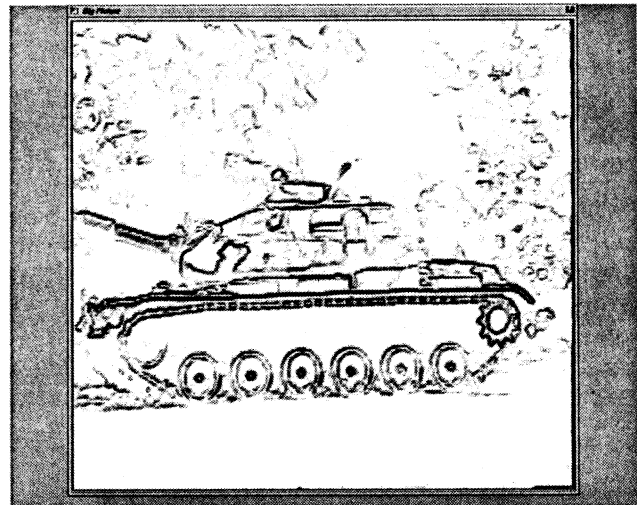
Fig. 8 Nonlinear resistive grid kernel approximation of a probability density function that contains a jump discontinuity.

nonlinear resistive grid have variable conductance values. By producing a conductance map of the resistive grid, a natural segmentation occurs, which can be seen in Figs. 9(b) and 10(b), corresponding to the input images Figs. 9(a) and 10(a), respectively. The dark areas in Figs. 9(b) and 10(b) correspond to drastically reduced conductance values produced by the nonlinearity inherent in the horizontal resistor circuits. Note that this segmentation produced by these reduced conductance values is part of the natural operation of the device. Also, these reduced conductance values serve to greatly limit the contribution of one texture type to the wavelet coefficients centered in an adjacent texture type—exactly the effect seen in Fig. 6(b).

The qualitative behavior of the nonlinear approach can best be illustrated with the help of a 1-D example. The top curve of Fig. 11 is a vertical slice down the center of the image, i.e., bushes to turret to tread to grass, depicted in Fig. 9(a). This slice crosses the three different textures of the tank image. As is apparent from an examination of the curve, some variance of signal structure exists in each of the three regions, however, most of the large jumps occur at the texture boundaries. The remaining curves in the figure portray the multiresolution approximation $L_j(x)$ to the original function at scale values of 2, 4, 8, 16, and 32. As is appropriate in a multiresolution approximation, we see a gradual loss of detail in the subsequent functional approx-



(a)



(b)

Fig. 9 (a) Tank image input to a nonlinear 2-D resistive grid and (b) the resultant conductance map for the tank image for a moderate nonlinearity setting. The conductance map has performed segmentation at all of the higher contrast boundaries.

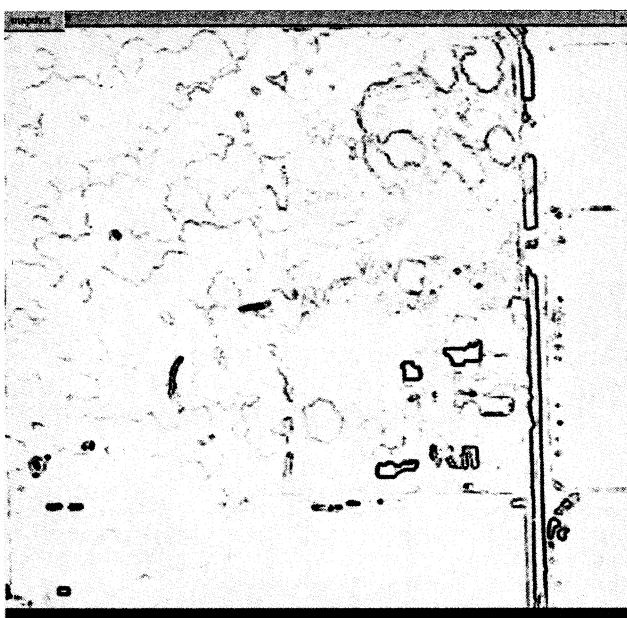
imations as we proceed from top to bottom in the figure. As discussed previously, we note that there is little mixing across texture boundaries in the multiresolution approximations.

Figure 12 shows the original function along with the wavelet coefficients $F_j(x)$ obtained by differencing L_j and L_{j-1} . These coefficients have a large magnitude in those regions where a large loss of signal detail exists between scale number i and $i-1$. As with the multiresolution approximations, the nonlinearity helps ensure the lack of contamination of these coefficients at the texture boundaries.

Next, we illustrate the actual texture features that are extracted from the wavelet coefficients. We seek to extract features that are relatively constant for a given texture type. Considering the deviations of $F_j(x)$ from a smoothed regression $v_j(x)$ of $F_j(x)$ (Fig. 13), a quantity analogous to the



(a)



(b)

Fig. 10 (a) Aerial image input to a nonlinear 2-D resistive grid and (b) the resultant conductance map for the aerial image for a moderate nonlinearity setting. The conductance map has performed segmentation at all of the higher contrast boundaries. The highest contrast boundaries are typically due to man-made sources.

local energy of the signal is obtained. Finally, we consider the deviations of the local energy $v_j(x)$ from a smoothed regression $v_{kk}(x)$ of $v_j(x)$ (Fig. 14). The $v_j(x)$ and $v_{kk}(x)$ determine a total of eight texture features. Preliminary discriminant analysis using these eight features indicates encouraging capabilities to distinguish the different classes of texture.

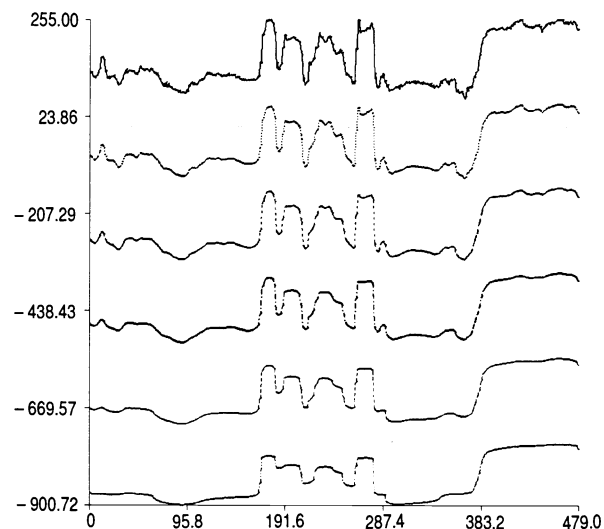


Fig. 11 Top to bottom: 1-D input (top line) produced by taking a vertical (turret to tread) slice of the tank image of Fig. 9(a); resistive grid outputs at successively doubled scales. Each output has been offset vertically for clarity.

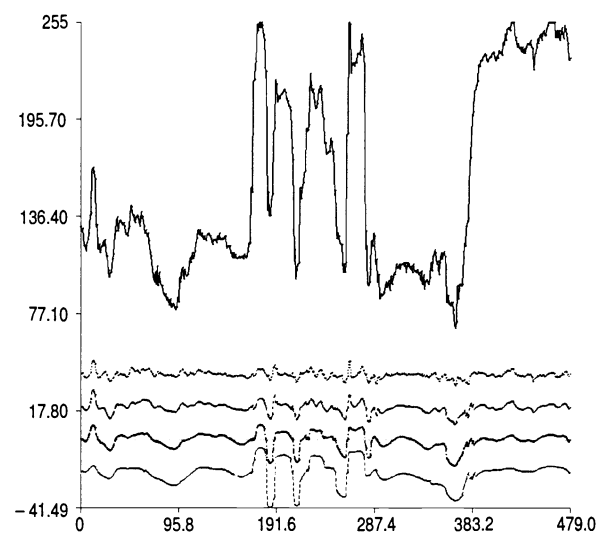


Fig. 12 Top to bottom: 1-D input (top line) produced by taking a vertical (turret to tread) slice of the tank image of Fig. 9(a); successive wavelet coefficients. Each output has been offset vertically for clarity. The input (top line) is the same as for Fig. 11.

To illustrate the full power of our approach, one more example will be discussed. As mentioned previously, many references have been made in the literature linking wavelets, texture analysis, and image segmentation. To fully illustrate this correspondence for our pseudowavelet approach, we need to study the nature of our derived energy features for several different texture types. This example details the performance of our approach on a set of homogeneous texture classes. Figure 15 is a 255 gray-level "texture quilt" consisting of 16 different textures. These textures originally appeared in a photographic album of textures by Brodatz.¹¹ A similar image has appeared previously in the literature in conjunction with the unsupervised texture discrimination work of Jain,¹² which uses Gabor filters. Each patch is 128×128 pixels for a total size of 512×512 .

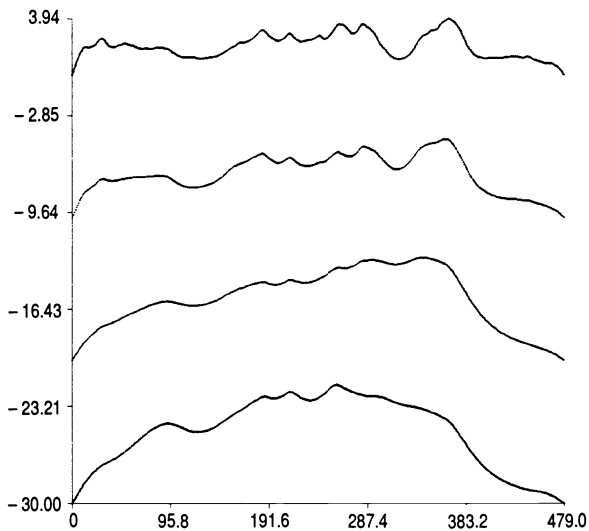


Fig. 13 Top to bottom: analog regression coefficients for increasing scale. Each output has been offset vertically for clarity.

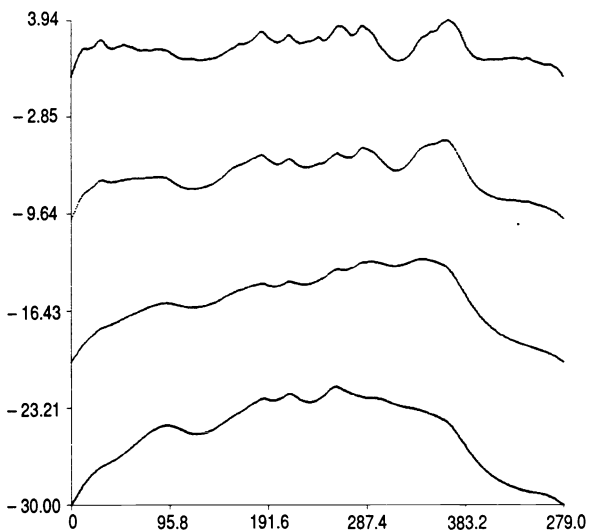


Fig. 14 Top to bottom: second-order analog regression coefficients for increasing scale. Each output has been offset vertically for clarity.

Figure 16 shows the degree of separation obtained for the 16 classes in a feature space derived from our eight first- and second-order energy variances. Each class is represented by 250 points randomly chosen in a 100×100 square positioned so its center is coincident with the center of the patch. As can be seen from Fig. 16, a high degree of separability exists for most of the classes. Nonparametric discriminant analysis results already show a marked improvement over results that have been obtained using traditional power law features, and the nonlinear segmentation effects appear to be central to these results.

Feature analysis has shown that the first- and second-order variance features are of equal relative importance in the texture discrimination. Note also that those classes that are overlapping in this projection can be separated in some of the other 3-D-derived feature spaces. In fact, it is our conjecture that near-perfect discrimination results could be

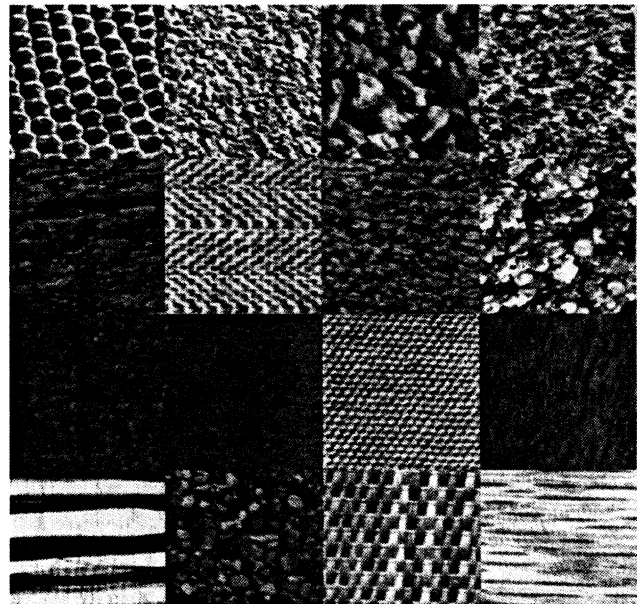


Fig. 15 Sixteen patch texture quilt. Numbered as shown in the diagram.

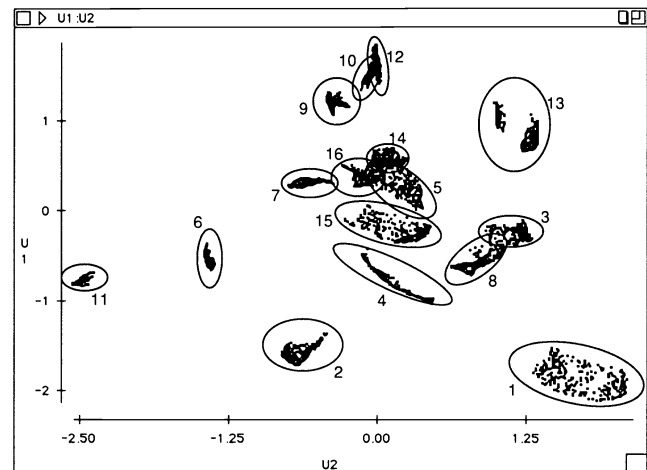


Fig. 16 Separation of the 16 quilt patches in a derived feature space.

obtained on these interior data sets using state-of-the-art classification procedures.

4 Conclusion

Our approach seems to be a powerful tool in identifying features useful in texture representation for (one type of) machine vision. Our approach differs from the standard wavelet approach in several key ways. First, we use an analog-derived exponential basis function. Second, we fully sample the resultant multiresolution approximations and wavelet coefficients. Third, we employ a nonlinear procedure to prevent contamination of features from nearby regions.

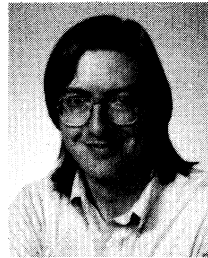
We have presented a hybrid optoelectronic design for near real-time processing to obtain wavelet coefficients and/or texture features. We have presented simulation results

that show that the nonlinear data-driven character of the wavelets obtained from nonlinear resistive grids can be an advantage rather than a disadvantage, especially where a high-contrast boundary separates different textures. The conversion of the wavelet coefficient maps to local power or variance features has been demonstrated to yield a useful set of features for texture discrimination.

Future work will address the need for the comparison of our technique with more conventional wavelet techniques for texture discrimination and image segmentation. This will be augmented by analytical work focusing on the nonlinear nature of our pseudowavelets.

References

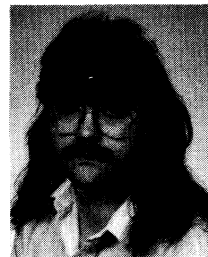
1. C. Mead, *Analog VLSI and Neural Systems*, Addison-Wesley, New York (1989).
2. S. G. Mallat, "A theory for multiresolution signal decomposition: the wavelet representation," *IEEE Trans. Patt. Anal. Mach. Intell.* **11**, 674–693 (1989).
3. J. L. Solka, C. E. Priebe, and G. W. Rogers, "An initial assessment of discriminant surface complexity for power law features," *Simulation*, May (1992).
4. C. E. Priebe, J. L. Solka, J. B. Ellis, and G. W. Rogers, "On discriminant surface complexity for power law features," submitted to *Patt. Recog.* (1992).
5. C. E. Priebe and D. J. Marchette, "Adaptive mixtures: recursive non-parametric pattern recognition," *Patt. Recog.* **24**, 1197–1209 (1991).
6. B. Julesz, "Textons the elements of texture perception and their interactions," *Nature* **290** (Mar. 1981).
7. T. Caelli, "Three processing characteristics of visual texture segmentation," *Spatial Vision* **1**, 19–30 (1985).
8. W. Poston, G. W. Rogers, C. E. Priebe, and J. L. Solka, "Resistive grid kernel estimator," submitted to *Patt. Recog. Lett* (1992).
9. S. G. Mallat and S. Zhong, "Complete signal representation with multi-scale edges," Technical Report 483, Courant Institute of Mathematical Sciences (1989).
10. J. M. Combes, A. Grossmann, and Ph. Tchamitchian, Eds. "Detection of abrupt changes in signal processing," in *Wavelets Time-Frequency Methods and Phase Space*, pp 99–101, Springer-Verlag, New York (1987).
11. P. Brodatz, *A Photographic Album for Artists and Designers*, Dover (1966).
12. A. K. Jain, "Unsupervised texture segmentation using Gabor filters," *Patt. Recog.* **24**, 1167–1186 (1991).



George W. Rogers received his BS degree from Georgia Southern College in 1977 and the PhD degree in theoretical physics from the University of South Carolina in 1984. Since 1985, he has been employed at the Dahlgren Division of the Naval Surface Warfare Center where he first worked in orbit computation and more recently in the field of artificial neural networks. His current research interests are in composite neuronal dynamics and adaptive pattern recognition.



Jeffrey L. Solka received his BS degree in mathematics and chemistry from James Madison University in 1978, his MS degree in mathematics from James Madison University in 1981, and his MS degree in physics from Virginia Polytechnic Institute and State University in 1989. Since 1984, Solka has been working in the areas of strategic defense, artificial neural systems, and pattern recognition for the Dahlgren Division of the Naval Surface Warfare Center.



Carey E. Priebe received his BS degree in mathematics from Purdue University in 1984 and his MS degree in computer science from San Diego State University in 1988. Priebe also did two years of undergraduate work at the U.S. Military Academy, West Point, and graduate work in mathematics at the University of California at San Diego. He is currently working toward a PhD in information technology (computational statistics) at George Mason University under the direction of Prof. Edward J. Wegman, with an expected conferral date of Spring 1993. Since 1985, Priebe has been working in adaptive systems and recursive estimators, first for the Naval Ocean Systems Center, San Diego, and since April of 1991, with the Naval Surface Warfare Center, Dahlgren, Virginia.

Harold H. Szu: Biography and photograph appear with the special section guest editorial.